

# PCCP

Accepted Manuscript



This is an *Accepted Manuscript*, which has been through the Royal Society of Chemistry peer review process and has been accepted for publication.

*Accepted Manuscripts* are published online shortly after acceptance, before technical editing, formatting and proof reading. Using this free service, authors can make their results available to the community, in citable form, before we publish the edited article. We will replace this *Accepted Manuscript* with the edited and formatted *Advance Article* as soon as it is available.

You can find more information about *Accepted Manuscripts* in the [Information for Authors](#).

Please note that technical editing may introduce minor changes to the text and/or graphics, which may alter content. The journal's standard [Terms & Conditions](#) and the [Ethical guidelines](#) still apply. In no event shall the Royal Society of Chemistry be held responsible for any errors or omissions in this *Accepted Manuscript* or any consequences arising from the use of any information it contains.

# Combining EXAFS spectroscopy and Molecular Dynamics simulations to understand the structural and dynamic properties of an Imidazolium Iodide Ionic Liquid

Valentina Migliorati,<sup>\*a</sup>, Alessandra Serva<sup>a</sup>, Giuliana Aquilanti,<sup>b</sup> Luca Olivi<sup>b</sup>, Sakura Pascarelli,<sup>c</sup> Olivier Mathon<sup>c</sup> and Paola D'Angelo<sup>\*a</sup>

Received Xth XXXXXXXXXXXX 20XX, Accepted Xth XXXXXXXXXXXX 20XX

First published on the web Xth XXXXXXXXXXXX 200X

DOI: 10.1039/b000000x

The structural properties of liquid 1-butyl-3-methylimidazolium iodide [C<sub>4</sub>mim]I have been investigated using an integrated approach that combines EXAFS spectroscopy and Molecular Dynamics (MD) simulations. A well defined first coordination shell composed on average of 4.5 I<sup>-</sup> ions around the imidazolium cation has been evidenced, and the structural arrangement of the I<sup>-</sup> ions has been found to be different in the proximity of the most acidic hydrogen atom of the imidazolium ring, as compared to the other two ring protons: in the former case the I<sup>-</sup> ion is not coplanar with the imidazolium ring plane, but it prefers to be above and below the plane itself, while in the latter the anion has the same probability of being or not being coplanar with the plane. A quantitative analysis of the I K-edge EXAFS spectrum of liquid [C<sub>4</sub>mim]I has been carried out starting from the structural information on the system derived from the MD simulation. This combined approach allows one to reduce the number of correlated model parameters required in the fitting of the experimental data and to increase the reliability of the EXAFS data analysis, that represents a non-trivial task when dealing with disordered systems. Moreover, the good agreement between the EXAFS experimental and theoretical spectra of liquid [C<sub>4</sub>mim]I has proven the reliability of the MD results and force field employed.

## 1 Introduction

Room-Temperature Ionic liquids (ILs) are systems consisting entirely of ions with melting points below 100 °C and exhibit many distinctive and valuable properties such as negligible vapor pressure, high thermal stability, non-flammability, wide electrochemical window, high ionic conductivity and tunable physical properties upon slight changes in their chemical architecture. From a physical chemistry point of view, the molecular origin of such unique properties is very interesting and defines a new class of condensed matter. ILs have received considerable attention from the scientific community over the past two decades due to their potential as environmentally friendly alternative to traditional organic solvents and for

their applications in many areas such as catalysis, synthesis, electrochemistry and sensoristics.<sup>1-9</sup>

Among ILs, alkyimidazolium iodides have extensively been considered as attractive alternatives to volatile organic solvents to be used as electrolytes in dye-sensitized solar cells (DSSCs). DSSCs are among the most extensively investigated devices that provide a high light-to-electric energy conversion yield.<sup>10</sup> One of the critical components of DSSCs is the electrolyte containing a I<sub>3</sub><sup>-</sup>/I<sup>-</sup> redox couple that mediates the dye regeneration process. High-efficiency solar cells typically use volatile organic solvents as electrolytes, which essentially preclude their use in outdoor applications because of the high vapor pressure of the solvents, and, in this context, alkyimidazolium iodides represent the ideal nonvolatile substitutes.<sup>11,12</sup>

Among iodide containing ILs, 1-butyl-3-methylimidazolium iodide, [C<sub>4</sub>mim]I, has been investigated by a number of experimental and computational techniques.<sup>13-19</sup> Using UV-Visible and Infrared spectroscopies in combination with DFT calculations, Shukla et al. investigated the reasons that make [C<sub>4</sub>mim]I liquid at room temperature while the analogous salts [C<sub>4</sub>mim]Cl and [C<sub>4</sub>mim]Br are solid.<sup>13</sup> The authors suggested that the hydrogen bonding interaction formed by the most "acidic" imidazolium ring

<sup>a</sup> Dipartimento di Chimica, Università di Roma "La Sapienza", P.le A. Moro 5, 00185 Roma, Italy. E-mail: [valentina.migliorati@uniroma1.it](mailto:valentina.migliorati@uniroma1.it), [p.dangelo@uniroma1.it](mailto:p.dangelo@uniroma1.it).

<sup>b</sup> Elettra-Sincrotrone Trieste S.C.p.A s.s. 14, km 163.5, I-34149 Basovizza, Trieste, Italy

<sup>c</sup> European Synchrotron Radiation Facility, BP 220 38043, Grenoble Cedex, France

† Electronic Supplementary Information (ESI) available: Figures S1-S9. Tables S1 and S2. Details on the analysis of [C<sub>4</sub>mim]I dynamic properties. See DOI: 10.1039/b000000x/

proton and the halide plays a predominant role in determining the physical state of the [C<sub>4</sub>mim]X ILs: going from Cl<sup>-</sup> to I<sup>-</sup> the C-H stretching band frequency was found to shift to higher wavenumbers as the hydrogen bonds become weaker and weaker, and the physical state of the [C<sub>4</sub>mim]X ILs from solid goes to liquid.<sup>13</sup> By combining Raman spectroscopy and Molecular Dynamics (MD) simulations Umebayashi and coworkers found similar structural trends for [C<sub>4</sub>mim]Cl, [C<sub>4</sub>mim]Br and [C<sub>4</sub>mim]I in the liquid phase, even if in the [C<sub>4</sub>mim]I IL the anion population facing the most acidic imidazolium ring proton decreases, being compensated by a population increase above and below the imidazolium ring plane.<sup>16</sup>

Despite these studies a detailed molecular level understanding of [C<sub>4</sub>mim]I is still missing, and due to the lack of suitable experimental techniques, no direct information on the interaction existing between the cation and the anion in liquid alkylimidazolium iodides has been obtained up to now. In this context X-ray absorption spectroscopy (XAS) is an experimental method that can provide accurate structural information on the local environment of the iodide anion. In particular extended X-ray absorption fine structure (EXAFS) spectroscopy has been found to be an innovative and efficient tool to gain structural information on ILs as it is one of the very few experimental techniques that furnishes direct information on the structural properties of disordered systems.<sup>20–25</sup>

Here, a combined approach using the EXAFS spectroscopy and MD simulations has been applied to study the I<sup>-</sup> local structure in liquid [C<sub>4</sub>mim]I. The structural and dynamic characterization of liquid samples is a very difficult task, and use of a unique method of investigation usually does not allow one to gain reliable information. Among other combined approaches, the use of simulation methods and XAS has been shown to be particularly well-suited to provide a reliable description of liquid samples.<sup>26–31</sup> The integrated MD-XAS approach allows one on the one hand to test the force fields used in the classical MD simulations, on the other hand to have reliable structural models to be used in the analysis of the EXAFS data. Moreover, this synergic procedure allowed us to have a global structural picture of the complex molecular organization of [C<sub>4</sub>mim]I both in proximity of the I<sup>-</sup> ion and in the longer distance range. We have recently combined MD and EXAFS to investigate the structural and dynamic properties of [C<sub>4</sub>mim]Br/water mixtures as a function of water concentration,<sup>32,33</sup> and here, for the first time, this powerful combined approach has been applied to the study of a pure liquid IL.

## 2 Methods

### 2.1 X-absorption measurements

[C<sub>4</sub>mim]I was purchased from Iolitec GmbH with a stated purity of > 99%. It was dried under vacuum for 24 hours and the final water content measured by Karl-Fischer titration was of 220 ppm. The I K-edge XAS spectra were collected in transmission mode at RT at the BM23 beamline of the European Synchrotron Radiation Facility ESRF. The monochromator was equipped with two flat Si311 crystals and in order to reduce harmonic contamination, which is weak in any case at the I K edge, the crystals were kept slightly detuned with a feedback system. The incident and transmitted fluxes were monitored by ionization chambers filled with Kr gas. The storage ring was operating in 2/3 fill mode with a typical current of 200 mA after refill. Measurements of liquid [C<sub>4</sub>mim]I were carried out at 300 K and the sample was kept in a cell with Kapton windows and a teflon spacer of 1 mm. To avoid contact with water the data acquisition was carried out keeping the cell under nitrogen flux.

### 2.2 EXAFS data analysis

The GNXAS program was used to calculate the EXAFS theoretical signals.<sup>34</sup> Phase shifts,  $A(k,r)$  and  $\phi(k,r)$ , have been calculated starting from the crystallographic structure<sup>35</sup> using muffin-tin potentials and advanced models for the exchange-correlation self-energy (Hedin-Lundqvist). For imidazolium ILs a new set of MT radii has been used that is 0.2, 0.9, 0.9 and 2.3 Å for H, C, N and I atoms, respectively. These radii correspond to an overlap between the iodine and hydrogen atoms of about 10 %.

Due to the structural disorder and to the high number of scattering atoms contributing to the total  $\chi(k)$  signal, rather than using the usual discrete form of the EXAFS equation, in this case the signal is modelled as a function of the radial distribution function  $g(r)$  as:

$$\chi(k) = \int_0^{\infty} dr 4\pi\rho r^2 g(r) A(k,r) \sin[2kr + \phi(k,r)] \quad (1)$$

where  $A(k,r)$  and  $\phi(k,r)$  are the amplitude and phase functions, respectively, and  $\rho$  is the density of the scattering atoms.  $\chi(k)$  theoretical signals are calculated by introducing the MD  $g(r)$ 's in Eq. 1 and the comparison between the experimental and theoretical curves allows one to assess the reliability of theoretical framework used in the simulations.

In particular, theoretical  $\chi(k)$  signals have been calculated both for the solid and liquid [C<sub>4</sub>mim]I using the MD I-HCR, I-HCW, I-H1, I-HC, I-CR, I-C1, I-CW and I-N  $g(r)$ 's obtained from the simulations. The contribution associated with the C2, CS and CT has been neglected, as the amplitude of the

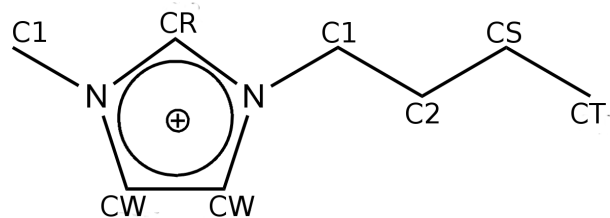


**Fig. 1** Atom labeling for the IL cation  $[\text{C}_4\text{mim}]^+$  as used in this article.

theoretical signals is very low. The atom labeling is shown in Figure 1. During the minimization procedure only two non structural parameters, namely the ionization threshold energy  $E_0$  and  $S_0^2$  are optimized.

### 2.3 Crystallographic structure of $[\text{C}_4\text{mim}]\text{I}$

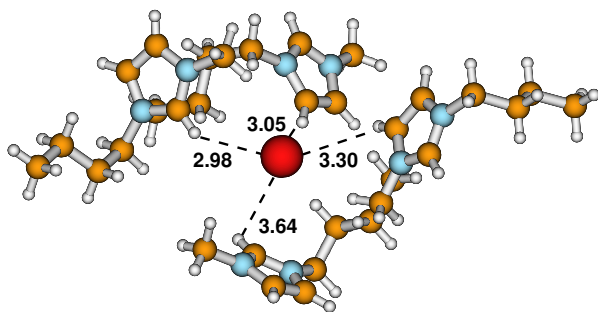


**Fig. 2** Local coordination around a single iodide ion in the crystal structure of  $[\text{C}_4\text{mim}]\text{I}$ ,<sup>35</sup> showing the close contacts between hydrogen atoms of cations and the anion. The iodine atom is in red, carbon in brown, nitrogen in cyan and hydrogen in white.

The crystal structure of  $[\text{C}_4\text{mim}]\text{I}$  indicates that anions and cations are interconnected by a weak network of hydrogen bonds that can be related to the observation that crystallization occurs at 233K.<sup>35</sup> In all crystal structures of  $[\text{C}_4\text{mim}]^+$  halides the butyl chain is commonly twisted out of the imidazolium ring plane at the position of butyl C1 atom (see Figure 1) and the N-C1-C2 bond angles are distributed in the narrow range 110-113°. The conformational feature of the cation that differentiates the crystal structures of the  $[\text{C}_4\text{mim}]^+$  halides is the torsion angles around C1-C2 in the butyl chains. In particular, in the  $[\text{C}_4\text{mim}]\text{I}$  crystal the butyl chain has a *gauche* conformation around the C1-C2 bond and *trans* conformation around the C2-CS bond. The HCR hydrogen atom is the only candidate to form a hydrogen bond with the iodide anion and although the CR-HCR...I angle is 132°, that is insufficient to form a hydrogen bond, the distance HCR-I is 2.98 Å. In Figure

2 the coordination geometry around the iodide ion is reported, while a full list of distances of all atoms within a cut-off distance of 4.0 Å from the iodide ion is reported in Table S1 of ESI†. In comparison to the existence of a bilayer structure observable in  $[\text{C}_4\text{mim}]\text{Br}$ , the crystal structure of  $[\text{C}_4\text{mim}]\text{I}$  shows a more disordered pattern and no  $\pi$ - $\pi$  stacking interactions between the aromatic rings seem to take place (see Figure S1 of ESI†). Indeed, the imidazolium rings lying in parallel planes are not stacked with each other in crystalline  $[\text{C}_4\text{mim}]\text{I}$ , but rather they undertake a completely staggered conformation.

### 2.4 Molecular Dynamics Details

MD simulations of  $[\text{C}_4\text{mim}]\text{I}$  have been carried out using the DL\_POLY package.<sup>36</sup> To simulate the liquid state, 500 molecules were placed in a cubic box, with periodic boundary conditions, and the size of the simulation box was chosen to reproduce the experimental density.<sup>37</sup> The force field parameters for the cation were taken from the Lopes and Padua force field,<sup>38,39</sup> which is one of the most widely used parametrizations in the area of IL modeling, and for the anion from OPLS,<sup>40</sup> and Lennard-Jones parameters for all of the different atoms were obtained from the Lorentz-Berthelot combining rules. The choice to combine OPLS with Lopes and Padua resides on the fact that these force fields are fully compatible with each other as the Lopes and Padua force field has been build starting from the OPLS one.<sup>38</sup> In particular, in the case of the imidazolium cation, the Lennard-Jones parameters for each atom type in the Lopes and Padua force field were taken from the OPLS-AA parametrization of heterocyclic aromatic rings or aliphatic compounds.<sup>38</sup> The Lennard-Jones parameters and partial atomic charges used in the present work are summarized in Table S2 of ESI†.

It is important to stress that partial atomic charges are typically obtained from electronic structure calculations of the isolated ions in vacuum with the constraint of integer net charges of  $\pm e$  on each ion, and this approach has been adopted also in the development of the Lopes and Padua force field. However, the atomic charges can affect dynamic properties and the model with unit positive and negative charges on the cation and the anion has been found to predict slower diffusion of the ions compared to experiment in liquid  $[\text{C}_4\text{mim}][\text{PF}_6]$ .<sup>41</sup> A possible strategy that has been proposed in the literature to overcome this problem is to employ fractional charges on the IL ions.<sup>41</sup> The reduction from the value of unity was rationalized as due to charge transfer between the ions and this procedure has proven to be beneficial for the simulation of transport properties. However, the advantage of the approach of Lopes and Padua is the generality of the force field that can be used for many ILs, while if one wants to simulate the ions with reduced charges a new set of partial atomic charges has to be

calculated for each cation-anion combination.

The initial configuration was constructed by positioning the IL cations and anions on selected lattice positions within a very large cubic simulation box. Extensive equilibration runs were performed, comprising 10000 steps of initial energy minimization and a NPT run at 300 K and very high pressure (100 atm) to compress the box volume until the experimental density was reached. Then the system was equilibrated under constant NVT conditions ( $T = 300$  K) for 10 ns. The production runs were carried out in the NVT ensemble for 10.2 ns, with a timestep of 1 fs and saving a configuration every 200 timesteps. The temperature was kept constant at 300 K using the Nosé-Hoover thermostat<sup>42,43</sup> with a relaxation constant of 0.5 ps. A cut-off of 12 Å was used to deal with nonbonded interactions, with the Ewald summation method to treat long-range electrostatic effects.<sup>44</sup> All of the bonds involving hydrogen atoms were constrained using the SHAKE algorithm. To confirm that our equilibration procedure led to a well-equilibrated liquid structure that did not depend on the initial configuration, a second configuration was obtained by melting the crystallographic structure (orthorhombic form)<sup>35</sup> and by modifying, during the equilibration run, the lengths of the three directions,  $a$ ,  $b$  and  $c$ , keeping them in a constant ratio, to reach the density of the liquid. Moreover, as it will be discussed later, in order to reach the diffusive regime of the system, another MD simulation was carried out at 400 K, while keeping the system density equal to that of the simulation at 300 K. The system was equilibrated under constant NVT conditions ( $T = 400$  K) for 1 ns. Also in this case the production runs were carried out in the NVT ensemble for 10.2 ns, with a timestep of 1 fs and saving a configuration every 200 timesteps.

To simulate the solid state, a crystal structure was generated by replicating the experimental unit cell<sup>35</sup> to create a box containing 500 pairs of  $[\text{C}_4\text{mim}]^+$  and  $\text{I}^-$  ions. This configuration was equilibrated during 1 ns at 233 K under constant NVT conditions, followed by production runs of 10.2 ns in the NVT ensemble at 233 K. All other parameters chosen to simulate the liquid state were also adopted for the solid system. No noticeable diffusion was observed, confirming the stability of the crystal with the force field. Figure 3 shows a pictorial representation of the simulation boxes used in the MD simulation of liquid  $[\text{C}_4\text{mim}]\text{I}$  starting from a random initial configuration and from the crystallographic structure, together with the MD simulation box of solid  $[\text{C}_4\text{mim}]\text{I}$ .

The structural properties of  $[\text{C}_4\text{mim}]\text{I}$  have been described in terms of radial, combined and spatial distribution functions. These analyses have been performed using the TRAVIS software developed by M. Brehm and B. Kirchner.<sup>45</sup> The dynamic properties of liquid  $[\text{C}_4\text{mim}]\text{I}$  have been also investigated starting from the MD simulation, and all details on the procedures used in the dynamic analyses are reported in ESI†.

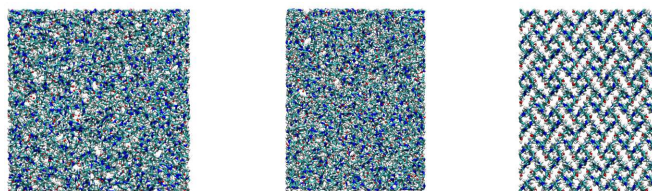


**Fig. 3** Pictorial representation of the simulation boxes used in the MD simulation of liquid  $[\text{C}_4\text{mim}]\text{I}$  starting from a random initial configuration (left panel), in the MD simulation of liquid  $[\text{C}_4\text{mim}]\text{I}$  starting from the crystallographic structure (middle panel) and in the MD simulation of solid  $[\text{C}_4\text{mim}]\text{I}$  (right panel).

## 3 Results

### 3.1 Radial distribution functions

In order to shed light on the structural properties of liquid  $[\text{C}_4\text{mim}]\text{I}$ , we have calculated the radial distribution functions  $g(r)$ 's of a selected subset of atoms from the MD trajectory and a series of coordination numbers,  $N$ , by integration of the radial distribution functions up to a selected cutoff. The general ordering of cations and anions in the system can be evinced from the looks of the Cation-Anion, Cation-Cation and Anion-Anion  $g(r)$ 's reported in Figure 4. Note that for the Cation the geometrical center of the imidazolium ring has been used in the  $g(r)$  computation. The Cation-Anion  $g(r)$  shows a well-defined first coordination shell, while Cation-Cation and Anion-Anion  $g(r)$ 's exhibit very broad features and no clear coordinations shells can be identified. The most interesting feature is the shoulder in the Cation-Cation  $g(r)$  at low distances, indicating that some imidazolium rings are arranged in such a way that their centers come as close as 5.0 Å. The Cation-Anion  $g(r)$  shows a distinct first peak at 5.1 Å and the coordination number of the first shell of  $\text{I}^-$  ions around a cation, choosing the cutoff distance as the position of the first minimum of the corresponding  $g(r)$  (6.1 Å), is 4.5. Additional insights into the ion coordination properties can be gained by defining an instantaneous Cation-Anion coordination number as the number of anions at a distance from the imidazolium cation shorter than the Cation-Anion  $g(r)$  first minimum, and analyzing its variation along the trajectory (see Figure S2 of ESI†). The results of this analysis show that a dominant percentage of cations are coordinated to either four or five anions, but there exists also a non-negligible percentage of 3-coordinated and 6-coordinated species.

In order to better characterize the local coordination of the iodide ion, we have calculated all of the  $g(r)$ 's involving the  $\text{I}^-$  ion from the MD trajectory. Looking at the  $g(r)$ 's reported in Figure 5 it is evident that the iodide ion is in closer contact with all of the hydrogen atoms, while the interactions with the

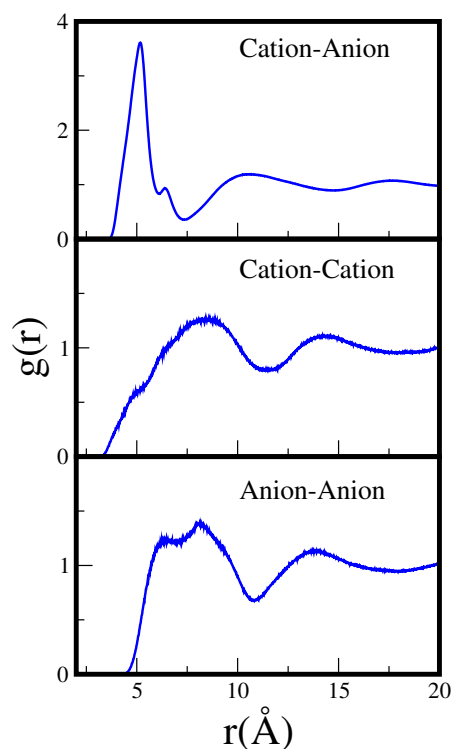


**Fig. 4** Radial distribution functions,  $g(r)$ 's, calculated from the MD simulation of liquid  $[\text{C}_4\text{mim}]\text{I}$ . Top panel: Cation-Anion  $g(r)$  calculated between the geometrical ring center of the  $[\text{C}_4\text{mim}]^+$  cation and the  $\text{I}^-$  ion. Central panel: Cation-Cation  $g(r)$ . Bottom panel: Anion-Anion  $g(r)$ .

carbon and nitrogen atoms are found at longer distances. In particular, the favorite sites of interaction of the anions are the hydrogen atoms of the imidazolium ring, HCR and HCW. In the I-HCR  $g(r)$  a first shell peak at  $3.3 \text{ \AA}$  is found and the coordination number is 2.0 if the integration is taken up to  $5.0 \text{ \AA}$ , cutoff value corresponding to the position of the  $g(r)$  first minimum. As concerns the interaction of the anion with the HCW atoms, a peak can be observed at  $3.3 \text{ \AA}$  and the coordination number, up to a distance cutoff of  $4.8 \text{ \AA}$ , is 3.4.

In order to assess the sensitivity of the EXAFS technique to the structural changes of  $[\text{C}_4\text{mim}]\text{I}$  in the crystal and liquid phases we have carried out a MD simulation of solid  $[\text{C}_4\text{mim}]\text{I}$  at  $233 \text{ K}$  and we have computed the theoretical EXAFS signals for both solid and liquid  $[\text{C}_4\text{mim}]\text{I}$ . In particular, starting from the MD  $g(r)$ 's we calculated the  $\chi(k)$  theoretical signals associated with all of the atoms surrounding the photoabsorber up to a cut-off distance of  $4.0 \text{ \AA}$  using Eq. 1. We have checked that the amplitude of the signals associated with higher distance shells is negligible. The comparison between the  $\chi(k)$  signals of the solid and liquid  $[\text{C}_4\text{mim}]\text{I}$  is shown in Figure 6, together with the corresponding MD  $g(r)$ 's. In all cases both

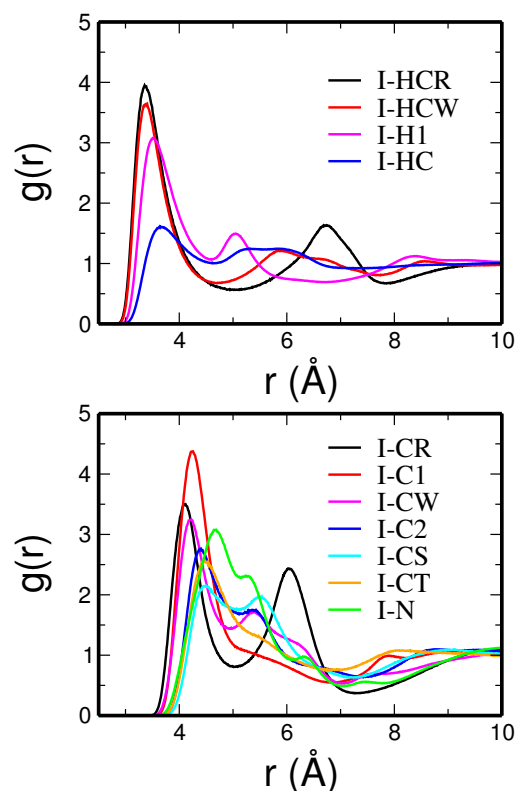


**Fig. 5** Radial distribution functions,  $g(r)$ 's, calculated from the MD simulation of liquid  $[\text{C}_4\text{mim}]\text{I}$ . In the upper panel the I-H  $g(r)$ 's are reported, while in the lower panel the I-C and I-N  $g(r)$ 's.

the amplitude and frequency of the EXAFS theoretical signals are different between solid and liquid phases. The total  $\chi(k)$  theoretical signals are compared in Figure S3 of ESI† showing once more that the EXAFS technique is sensitive to the structural differences highlighted by the MD simulations. These signals have been obtained by adding all of the contributions of Figure 6 for both liquid and solid  $[\text{C}_4\text{mim}]\text{I}$ .

### 3.2 EXAFS analysis of the liquid $[\text{C}_4\text{mim}]\text{I}$

The I K-edge EXAFS spectrum of liquid  $[\text{C}_4\text{mim}]\text{I}$  has been collected at room temperature. This experimental data can be analysed starting from the  $\chi(k)$  theoretical signal calculated from the  $g(r)$ 's obtained from the MD simulation. In particular, a direct comparison between the local coordination geometry of the  $\text{I}^-$  ion obtained from the MD calculations and EXAFS data allows on the one hand to properly interpret the experimental spectra, on the other to assess the reliability of the simulations. As previously mentioned  $\chi(k)$  theoretical signals have been calculated using Eq. 1, starting from the I-HCR, I-HCW, I-HC, I-H1, I-C1, I-CW and I-CR  $g(r)$ 's cal-

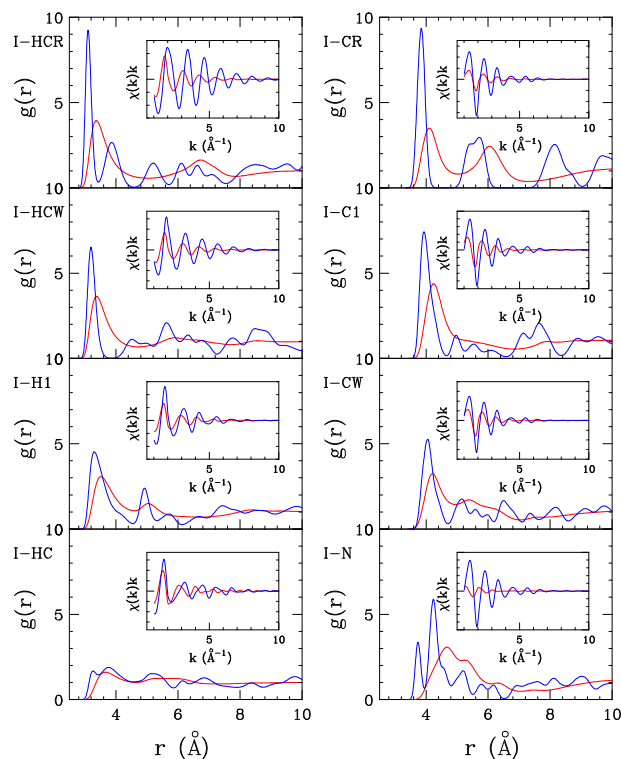


**Fig. 6** Radial distribution functions,  $g(r)$ 's, calculated from the MD simulations of solid (blue lines) and liquid (red lines)  $[\text{C}_4\text{mim}]\text{I}$ . The insets show theoretical EXAFS signals calculated from the MD  $g(r)$ 's.

culated from the MD trajectory for liquid  $[\text{C}_4\text{mim}]\text{I}$ . We have also calculated the  $\chi(k)$  theoretical signals associated with the nitrogen atoms of the cation and these atoms have been found to provide a negligible contribution to the total EXAFS signal. The MD structural parameters were kept fixed during the analysis and the results of the EXAFS analysis are shown in Figure 7. In the upper panel, the first seven curves from the top are the I-H and I-C theoretical signals, while the remainder of the figure shows the total theoretical contribution in comparison with the experimental spectrum. Least-squares fits of the EXAFS spectra were performed in the range  $k=2.3\text{--}12.0 \text{ \AA}^{-1}$  and minimization procedures were applied only to the nonstructural parameters to improve, as far as possible, the agreement between calculated signals and experimental spectra. From the minimization procedure  $E_0$  was found to be 9 eV above the first inflection point of the spectrum, while  $S_0^2$  was found equal to 0.8. Overall, the agreement between theory and experiment is very good proving that the structural information derived from the MD simulation is reliable, and that the chosen force field is capable of providing a correct description of the system. In the lower panel of Figure 7 the comparison

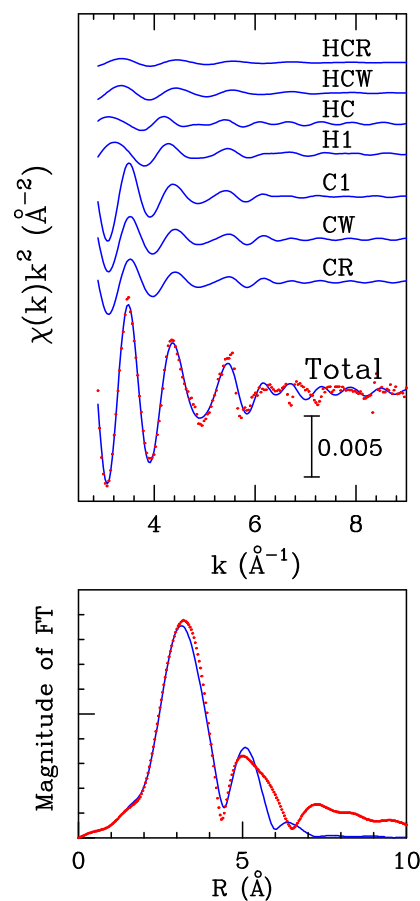


**Fig. 7** Upper panel: Comparison between the EXAFS experimental spectrum of liquid  $[\text{C}_4\text{mim}]\text{I}$  (dotted red line) and theoretical signals (solid blue line) calculated from the I-HCR, I-HCW, I-HC, I-H1, I-C1, I-CW and I-CR MD  $g(r)$ 's. Lower panel: Nonphase-shifted corrected Fourier transforms of the experimental data (dotted red line) and of the theoretical signal (solid blue line).

between the nonphase-shifted corrected Fourier transforms of the experimental data and of the theoretical signal is reported and, as it can be seen, a very good agreement is found also in distance space.

### 3.3 Combined distribution functions

Once the validity of the MD structural results has been assessed on the basis of the EXAFS experimental data, additional information on the three-dimensional arrangement of ions in liquid  $[\text{C}_4\text{mim}]\text{I}$  can be obtained from the analysis of the MD trajectory. In particular, the interaction of the iodide ions with the HCR and HCW hydrogen atoms of the imidazolium ring can be analyzed studying the combined distribution functions (CDFs) that combine two functions, namely the

radial and angular distribution functions (ADFs). Normally, we would have put the  $g(r)$  and ADF values into linear histograms. Conversely, we regard the two values as 2-tuple, so that they are connected and related to each other as they stem from the same configuration. The obtained 2-tuple is put into a two dimensional histogram. All of the CDFs calculated from the MD simulation of liquid  $[\text{C}_4\text{mim}]\text{I}$  are depicted in Figure 8. Figure 8A shows the CDF obtained combining the  $g(r)$  between the HCR atom of  $[\text{C}_4\text{mim}]^+$  and the  $\text{I}^-$  ion and the distribution function of the angle between the CR-HCR vector in  $[\text{C}_4\text{mim}]^+$  and the CR-I vector. This angle is labeled as  $\omega_{\text{HCR}}$  and shown in Figure S4 of ESI†. One can see that for a distance of about 3.17 Å the region of maximum intensity is between 20° and 40°, which corresponds to a configuration where the  $\text{I}^-$  ion is not located in front of the CR-HCR vector but forms an angle of about 30° with this vector. The second CDF (Figure 8C) is obtained combining the  $g(r)$  between the HCR atom of  $[\text{C}_4\text{mim}]^+$  and  $\text{I}^-$  ion and the ADF calculated using the angle formed between the normal vector to the ring plane and the intermolecular ring center-I vector (see Figure S4 of ESI†). In this case for the distance range around 3.0 Å a symmetric function is found, with a minimum at 90° and two maxima centered at about 50° and 130°: the tendency of the iodide is not to be coplanar with the plane of the imidazolium ring but to form with it an angle of about 40°. Then CDFs considering the interaction of the anion with the HCW hydrogen atoms have been calculated. In the first CDF (see Figure 8B) we have considered the distance between the HCW atom and  $\text{I}^-$  ion and the angle,  $\omega_{\text{HCW}}$ , between the CW-HCW and the CW-I vectors. It can be seen a low intensity maximum at 20° and a distance of about 3.0 Å indicating that the anion tends to form an angle of 20° with the CW-HCW vector. In the second CDF, depicted in Figure 8D, it has been considered the HCR-I  $g(r)$  with the angle between the normal vector to the ring plane and the ring center-I vector. The highest correlation is found between 60° and 120°: the anion has the same probability of being either coplanar to the imidazolium ring plane or not. Therefore, our CDF analysis shows that the interactions of the anion with the HCR and HCW hydrogen atoms are different. In both cases the  $\text{I}^-$  ion is not located in front of the C-H vector, and this is particularly true in the case of the HCR atom (Figure 8A shows a larger area of higher intensity as compared to Figure 8B). In the vicinity of the HCR atom, the  $\text{I}^-$  ion has a minimal chance of being coplanar to the ring plane and a higher probability of being above and below the plane itself, while for the HCW atoms the probability of being or not being coplanar with the plane is similar.

### 3.4 Spatial distribution functions

The three-dimensional arrangement of the anions around the imidazolium cation can be observed looking at the spatial dis-

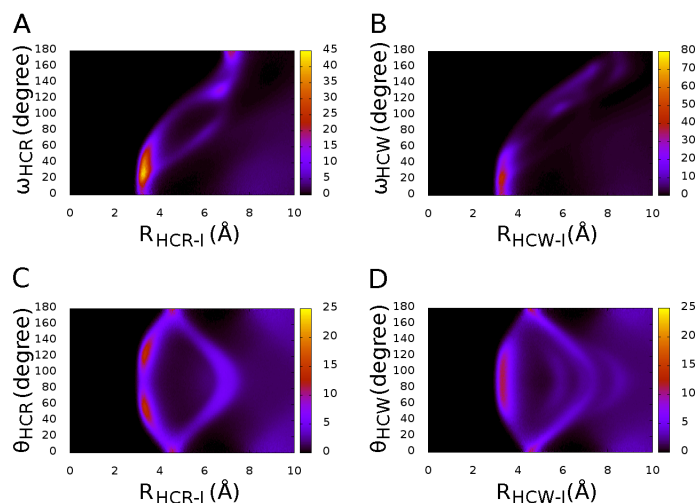


**Fig. 8** Combined distribution functions (CDFs) calculated from the MD simulation of liquid  $[\text{C}_4\text{mim}]\text{I}$ . (A) CDF showing the correlation between the HCR-I  $g(r)$  (x-axis) and ADF of the angle between the CR-HCR and CR-I vectors (y-axis). (B) CDF showing the correlation between the HCW-I  $g(r)$  (x-axis) and ADF of the angle between the CW-HCW and CW-I vectors (y-axis). (C) CDF showing the correlation between the HCR-I  $g(r)$  (x-axis) and ADF of the angle between the normal vector to the ring plane and the intermolecular ring center-I vector (y-axis). (D) CDF showing the correlation between the HCW-I  $g(r)$  (x-axis) and ADF of the angle between the normal vector to the ring plane and the intermolecular ring center-I vector (y-axis).

tribution functions (SDFs) shown in Figure 9. The SDFs have been calculated from the MD simulation and the isodensity surfaces of the  $\text{I}^-$  ion are colored magenta. The association between anions and cations is predominantly driven by interactions of the  $\text{I}^-$  ion with the hydrogen atoms of the imidazolium ring, HCR and HCW, especially with HCR because it is the most acidic hydrogen atom. On the contrary, the approach of the anion toward the cation from the side of the alkyl chains is inhibited due to their steric hindrance. The first evident result of the SDF analysis is that the  $\text{I}^-$  ion that interacts with the HCR atom is not coplanar with the imidazolium ring plane, but it prefers to be above and below the plane itself (Figure 9A). In the case of the HCW atoms the  $\text{I}^-$  distributions are less broad as compared to the distributions in the proximity of HCR. Moreover, the isosurfaces are shifted towards the lateral chains and the shift is more pronounced for the anions close to the methyl group, as a result of the decreased steric hindrance of the methyl group as compared to the butyl chain (Figure 9B). Furthermore, the anion near the HCW atoms can be also coplanar with the imidazolium ring plane. Figure 9C shows that the anion accessible region, close to the HCR atom, is

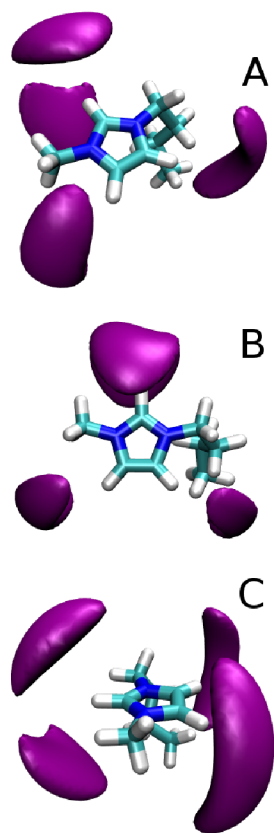


**Fig. 9** Spatial distribution functions (SDFs) of the anions (magenta) around the cation, calculated from the MD simulation of liquid  $[\text{C}_4\text{mim}]\text{I}$ . A, B and C panels show three different orientations of the system.

larger than that near the HCW atoms, and in the vicinity of HCR there is a higher penetration into the space surrounding the normal to the ring plane. Finally, Figure S5 of ESI† shows the favored surfaces for the close-by cations around a single imidazolium cation (blue), overlaid on the SDF of the anions (magenta). The cations tend to fill the area not occupied by the anions and, in particular, a large cation distribution can be observed in front of the CR-HCR vector. Both the spatial and the combined distribution functions have shown that  $\text{I}^-$  ions when interacting with the most acidic hydrogen atom HCR have a high probability of being above and below the imidazolium ring plane and a very low probability to be coplanar with the plane itself. This trend is opposite to that shown from MD simulations of pure  $[\text{C}_4\text{mim}]\text{Br}$  IL carried out under high temperature<sup>46,47</sup> and from a MD study of  $[\text{C}_4\text{mim}]\text{Br}/\text{water}$  mixtures with different molar ratios.<sup>32</sup> In order to understand the different structural behavior of the two halides, the  $\text{I}^-$  and  $\text{Br}^-$  size has to be considered: in the former case, the anion has a larger ionic radius and prefers not to be coplanar with the

ring plane, in the latter, the anion is smaller and it is located in the plane. This result is in line with the one obtained from a combined UV-Visible, IR and DFT study of  $[\text{C}_4\text{mim}]\text{X}$ .<sup>13</sup> The anion position was found to be crucial in determining whether an IL is liquid at ambient temperature or not. The  $\text{Cl}^-$  and  $\text{Br}^-$  ions are located in the imidazolium ring plane and, because of their small size, there is compact packing of ions in the crystal lattice leading to higher melting points. On the contrary, due to the larger size of the iodide anion, it does not fit well in the lattice, leading to a liquid state at ambient temperature.<sup>13</sup>

### 3.5 Convergence analysis of the structural properties

Generally, in MD simulations ILs are characterized by slow dynamics. As a consequence, it is essential to check the convergence of the structural properties obtained from the MD trajectories to be sure that the phase space of the system has been correctly sampled. To this purpose the trajectory obtained from the MD simulation of liquid  $[\text{C}_4\text{mim}]\text{I}$  was divided into different time slices and the behaviour of the structural properties was monitored as a function of the time slices. As concerns all of the structural properties analyzed in this work, we have found that a MD time interval of 0.5 ns is enough to reach convergence. Figure S6 of ESI† shows, as an example, the Cation-Anion  $g(r)$ 's calculated in six different time slices of 0.5 ns and the  $g(r)$  obtained from the entire trajectory, and, as it can be seen, all of the  $g(r)$ 's are identical.

Moreover, in order to demonstrate that we have properly sampled the phase space, the liquid  $[\text{C}_4\text{mim}]\text{I}$  system has been simulated starting from a different initial configuration, as described in the Methods section. In particular, in the former case, the initial configuration was built by positioning the IL cations and anions on randomly selected lattice positions within a very large cubic simulation box. In the latter, it was obtained by melting the crystallographic structure (orthorhombic form) and by modifying the lengths of the three directions,  $a$ ,  $b$  and  $c$ , to reach the density of the liquid. The  $g(r)$ 's have been calculated from the MD trajectory and they have been compared with those obtained from the first simulation. In Figure S7 of ESI† we show, as an example, the Cation-Anion  $g(r)$ 's, calculated both for the simulation carried out starting from a random initial configuration and for that obtained from the crystallographic structure. The  $g(r)$ 's obtained from the analysis of this system are in perfect agreement with those calculated previously, and therefore we can be confident that the structural properties do not depend on the initial configuration of the system.

### 3.6 Dynamic properties: Self-Diffusivity

A thorough study of the microscopic dynamics of ILs is important for better understanding their chemical reactivity, elec-

trical conductivity and mass transfer. These properties play an important role in applications of ILs as alternative solvents, propellants and conductors. When evaluating the dynamic properties of these systems, besides checking the convergence of the results, it is essential to be sure that a diffusive regime has been reached during the MD simulation. Because of the sluggish dynamics of ILs, in order to probe diffusive behavior, the simulation times must be quite long. In our simulation 10.2 ns production runs were used. One way to test if the simulations are long enough to probe diffusive behavior is to compute, from the ion mean square displacement, a linearity parameter  $\beta(t)$  (see Ref.<sup>48</sup> for its definition) that must approach unity in the diffusive regime. At values below  $\beta(t)=1$ , the system is in the subdiffusive regime and any apparent self-diffusivity will underestimate the true self-diffusivity. We have seen that on a time scale of a few femtoseconds  $\beta(t)$  is close to 2; then the system is in the subdiffusive regime and  $\beta(t)$  increases linearly until reaching a value of about 0.9. Although the simulation is rather long the diffusive regime has not been reached since a value of  $\beta(t)=1$  is not achieved even after 10.2 ns of simulation. For this reason, in order to probe diffusive regime, we have carried out a new MD simulation of liquid [C<sub>4</sub>mim]I at high temperature (400 K), while keeping the system density equal to that used in the simulation at 300 K. The  $g(r)$ 's have been calculated from the 400 K MD trajectory to understand if the increase of temperature affects not only the dynamic properties, as expected, but also the structural ones. In Figure S8 of ESI† we show the Cation-Anion  $g(r)$ 's calculated from the two simulations carried out at 300 K and 400 K. The  $g(r)$ 's are identical and this result indicates that the structural properties do not change with increasing temperature, provided that the system density is kept unchanged. Moreover, at this temperature  $\beta(t)$  approaches unity after 1 ns of simulation ensuring that the system is in the diffusive regime and the dynamic properties calculated from the MD trajectory can be regarded as reliable. The fact that the structural properties are identical for both simulations guarantees that, from a structural point of view, the phase space is correctly sampled even if the system is not in a diffusive regime.

### 3.7 Dynamic properties: Convergence Analysis

It is worthwhile to check the convergence of the dynamic properties calculated from the MD trajectories, but, at variance with the convergence analysis of the structural properties, in this case the convergence depends on the time scale of the particular motion under investigation. For properties with relaxation times shorter than 5 ps the convergence of the corresponding correlation function was reached in a few hundred picoseconds of MD trajectory. An example can be seen in Figure S9A and S9B of ESI†, where the correlation functions

of Cation-Anion ion-pair dynamics are depicted. In particular, in panel A the correlation function has been calculated in three time slices of 0.3 ns and from the entire MD trajectory carried out at 300 K, while in panel B the function has been calculated in three time slices of 0.1 ns from the 400 K MD simulation. As concerns motions with relaxation times shorter than 100 ps, 3 ns of MD simulation can be considered enough to reach convergence, as shown in Figure S9D of ESI†. When the relaxation times are comprised in the range 100 to 400 ps, the convergence is reached in almost 5 ns and Figure S9C of ESI† shows, as an example, the correlation function of Cation-Anion ion-cage dynamics calculated in two different time slices of 5 ns. In this case the curves are not completely overlapped, and the integral calculated for each of them differs by about 20 ps. Generally, to have a good statistics, a correlation function should be calculated in a time interval at least double to the one in which the function goes to zero. This is not the case since the correlation function goes to zero after about 5 ns and so we do not have a time interval long enough to have a good statistics of the calculation of the function in the different time slices. In this case only the order of magnitude of the relaxation times calculated from the MD simulation can be considered as reliable. Finally, for dynamic properties that take place on longer time scale it is not possible to make a proper convergence analysis as the corresponding correlation functions decay too slowly and the relaxation times can be only regarded as a lower limit.

### 3.8 Dynamic properties: Results

Table 1 shows the results of the dynamic properties calculated from the MD simulations of liquid [C<sub>4</sub>mim]I at 300 K and 400 K. The translational diffusion coefficients of both anions and cations were computed and for both ions the coefficients increase with increasing temperature. The [C<sub>4</sub>mim]<sup>+</sup> and I<sup>-</sup> diffusion coefficients calculated from our simulations are in the same order of magnitude of the coefficients obtained from recent MD simulations of liquid [C<sub>4</sub>mim]I at 358 K.<sup>18</sup> Moreover, for the anion slightly lower values have been obtained than for the cation at both temperature values. This trend is the same as the one obtained from MD simulations of [C<sub>4</sub>mim]I, [C<sub>6</sub>mim]I, [C<sub>8</sub>mim]I at 358 K<sup>18</sup> and of pure [C<sub>4</sub>mim]Br IL carried out under high temperature conditions.<sup>46</sup> Our results are also in agreement with a previous MD investigation of [C<sub>4</sub>mim][BF<sub>4</sub>] showing that in the pure IL the anion moves slower than the cation, while in water mixtures the anion diffusion coefficient becomes higher than the cation one.<sup>49</sup> In line with the latter result, faster translational motion for halide ions as compared to [C<sub>4</sub>mim]<sup>+</sup> cations has been obtained also in our MD investigation of [C<sub>4</sub>mim]Br/water mixtures with different molar ratios.<sup>32</sup>

The reorientational motion of imidazolium cations was in-

investigated by considering the rotation of the normal to the ring plane and the time constants obtained are reported in Table 1. The reorientational correlation time decreases as the temperature increases and this means that the increase of temperature makes the rotational motions faster. Moreover, at 300 K the time constant should be considered only a lower limit since it is of the same order of magnitude of the MD simulation time. We have also noticed that the cation reorientational time at 400 K is significantly higher as compared to the cation reorientational time recently calculated by Kohagen et al. from MD simulations of pure [C<sub>4</sub>mim]Br carried out at the same temperature.<sup>47</sup>

Finally, the ion-pair and ion-cage dynamics have been investigated by computing the relaxation times of continuous correlation functions as described in ESI†. In the ion-pair dynamics we only counted the next neighboring anion at each time with respect to the ring center of one particular cation, while for the ion-cage dynamics all anions that are within a selected cutoff distance around the ring center are taken into account. All values calculated from the MD simulations are reported in Table 1. As expected, both for ion-pair and ion-cage dynamics the relaxation times decrease as the temperature increases showing that the temperature has the tendency to make the dynamics of the system faster. In the presence of ion pairs the correlation times calculated according to both definitions should be of the same order of magnitude.<sup>47</sup> By applying the stricter ion-cage definition (continuous), we obtain a correlation time for the ion-pair dynamics which is 2 order of magnitude smaller than the correlation time for the ion-cage definition and this difference holds for the two investigated temperatures. This result is a clear indication that the ions in pure ILs exist in a fluctuating network and not as separated ion pairs. Thus, the ion-cage dynamics describes the distortion of an ion-cage and not the breaking of an ion pair. Moreover, the relaxation time of the continuous time correlation function for the ion-cage dynamics is significantly shorter than the relaxation time of the ring reorientation, meaning that the reason for the breaking of a cation-anion cage could be the translational movement and not the reorientation of the imidazolium ring. This behaviour is in agreement with the results of previous MD simulations of [C<sub>4</sub>mim]Br/water mixtures with different molar ratios<sup>32</sup>. On the contrary, our result is opposite to that shown from a MD simulation of pure [C<sub>4</sub>mim]Br, where the relaxation times for the ion-cage dynamics and for the ring reorientation are on the same time scale for the whole investigated temperature range.<sup>47</sup> To analyze the ion-cage dynamics we have also used an intermittent time-correlation function defined in ESI†. The relaxation time of this function (see Table 1) has been calculated considering that the criteria which define an aggregate species can be unaccomplished for a time interval up to 1 ps. The intermittent ion-cage dynamics both at 300 K and 400 K shows signifi-

	300 K	400 K
Diffusion coefficients		
$D_{Anion}$	0.37	1.38
$D_{Cation}$	0.45	1.67
Rotational Dynamics		
$\tau_{Cation}$	1601.7	383.9
Ion-Cage Dynamics		
$\tau_C$	242.8	89.5
$\tau_I$	983.0	377.3
Ion-Pair Dynamics		
$\tau_C$	2.7	1.6

**Table 1** Diffusion coefficients of anions and cations; relaxation times of correlation functions for rotational dynamics of cations ( $\tau_{Cation}$ ), for the continuous ( $\tau_C$ ) and intermittent ( $\tau_I$ ) ion-cage dynamics and for the ion-pair dynamics of cation-anion interaction. See ESI† for the definition of the different correlation functions. Diffusion coefficients are expressed in  $10^{-7}$  cm<sup>2</sup>/s and all relaxation times are expressed in ps.

cantly larger correlation times than those for the continuous dynamics. Moreover, the relaxation time of intermittent correlation functions can be regarded as a sort of residence time of the anions in the coordination sphere of the cation and vice versa.

### 3.9 Discussion and Conclusions

In this work a thorough characterization of the structural properties of liquid [C<sub>4</sub>mim]I has been carried out using an integrated approach that combines EXAFS spectroscopy and MD simulations. From a structural point of view, a well defined first coordination shell of I<sup>-</sup> ions around the imidazolium cation has been found from the analysis of the MD trajectory. This coordination shell is composed on average of 4.5 I<sup>-</sup> ions, even if instantaneously the anion-cation coordination number can take a value in the range between 2 and 7. The favorite interaction sites of the anions are the hydrogen atoms of the imidazolium ring, and a very interesting result is that the structural arrangement of the I<sup>-</sup> ions is different in the proximity of HCR and of the two HCWs: the I<sup>-</sup> ion that interacts with the HCR atom is not coplanar with the imidazolium ring plane, but it prefers to be above and below the plane itself, while in the vicinity of the HCW atoms I<sup>-</sup> has the same probability of

being or not being coplanar with the ring.

In this work we have carried out, for the first time, the quantitative analysis of the I K-edge EXAFS spectrum of a pure liquid IL, starting from the microscopic description of the system derived from a MD simulation. The importance of combining MD and EXAFS is now well recognized and allows one to obtain very accurate structural information on disordered systems that represent a quite challenging subject to be treated. The very good agreement between theory and experiment that we obtained here proves that the structural information derived from the MD simulation is reliable, and that the chosen force field is able to provide a correct description of the system from a structural point of view. This is an important result since the combined EXAFS-MD approach is a very strict test of the quality of the potentials used in the simulations, and, without such a comparison, the reliability of the MD structural results is hardly provable. This is because empirical potentials are not always able to provide a correct description of structural, energetic, and dynamic properties of systems different from the specific experimental properties for which they have been developed.

On the other hand the synergic use of EXAFS and MD allowed us to carry out a reliable analysis of the EXAFS spectrum. This is not a trivial task when the EXAFS technique is applied to the study of disordered systems, due to the numerous and strongly correlated parameters involved in the fitting of the experimental data. The number of fitting parameters could become quite high in some cases, thus exceeding the number of independent points according to the Nyquist theorem. In the EXAFS analysis carried out here, all of the hydrogen atoms and three of the carbon atoms (CR, CW and C1) of the imidazolium cation have been found to provide a detectable contribution to the EXAFS spectrum. Therefore, a high number of fitting parameters should be used if the standard EXAFS analysis using different coordination shells around the photoabsorber atom is carried out. A possible solution of this problem is to use in the EXAFS analysis the structural information derived from MD simulations, without carrying out any optimization in the structural parameter space. In this respect, the original application of EXAFS and MD simulations used in the present research paves the route for the systematic use of an integrated approach, with increased reliability, in the structural investigation of ILs.

A last remark we would like to make concerns the procedure we used to calculate the theoretical EXAFS spectrum of solid [C<sub>4</sub>mim]I starting from an MD simulation of the system. It is important to point out that thermal disorder significantly affects the EXAFS spectrum, being usually responsible for up to 20-80% of the total amplitude. Therefore, a reasonable estimate of the atomic thermal motion in the EXAFS spectra is crucial for the analysis, but still remains an unresolved issue. In the conventional EXAFS analysis of crystalline samples us-

ing peak fitting approaches the Debye Waller factors can be fitted against experimental data but this largely increases the number of fitting parameters that, as previously mentioned, is limited by the number of independent data points. A possible strategy to overcome this problem is to calculate the EXAFS signal by describing the atomic thermal motion of the solid sample in terms of  $g(r)$ 's obtained from a MD simulation, thus reducing the number of correlated fitting parameters and increasing the reliability of the EXAFS analysis. While this approach has been widely used in the past for the study of liquid samples, it has been hardly applied to solids. In the case of ILs due to the disordered structure incidental to the nature of these systems, this approach turns out to be essential to carry out a reliable analysis of the EXAFS experimental data.

## Acknowledgments

We acknowledge the European Synchrotron Radiation Facility for provision of synchrotron radiation facilities and we would like to thank the staff of BM23 for assistance in using the beamline. This work was supported by the CINECA supercomputing centers through the grant IscrC.COLACIL (n.HP10CCQEUQ).

## References

- 1 M. Freemantle, *An Introduction to Ionic Liquids*, RSC Publishing, 2009.
- 2 *Ionic Liquids IIIA: Fundamentals, Progress, Challenges, and Opportunities: Properties and Structure*, ed. R. Rogers and K. Seddon, American Chemical Society, Washington D.C., 2005, vol. 901.
- 3 V. Migliorati, P. Ballirano, L. Gontrani, A. Triolo and R. Caminiti, *J. Phys. Chem. B*, 2011, **115**, 4887–4899.
- 4 *Ionic Liquids IIIB: Fundamentals, Progress, Challenges, and Opportunities: Transformations and Processes*, ed. R. Rogers and K. Seddon, American Chemical Society, Washington D.C., 2005, vol. 902.
- 5 V. Migliorati, P. Ballirano, L. Gontrani and R. Caminiti, *J. Phys. Chem. B*, 2012, **116**, 2104–2113.
- 6 R. D. Rogers and K. R. Seddon, *Science*, 2003, **302**, 792–793.
- 7 P. D'Angelo, A. Zitolo, V. Migliorati, E. Bodo, G. Aquilanti, J. L. Hazemann, D. Testemale, G. Mancini and R. Caminiti, *J. Chem. Phys.*, 2011, **135**, 074505.
- 8 L. Gontrani, E. Bodo, A. Triolo, F. Leonelli, P. D'Angelo, V. Migliorati and R. Caminiti, *J. Phys. Chem. B*, 2012, **116**, 13024–13032.
- 9 A. Zitolo, V. Migliorati, G. Aquilanti and P. D'Angelo, *Chem. Phys. Lett.*, 2014, **591**, 32–36.
- 10 B. Regan and M. Grätzel, *Nature*, 1991, **353**, 737–740.
- 11 P. Bonhote, A.-P. Dias, N. Papageorgiou, K. Kalyanasundaram and M. Grätzel, *Inorg. Chem.*, 1996, **35**, 1168–1178.
- 12 N. Papageorgiou, Y. Athanassov, M. Armand, P. Bonhote, H. Pettersson, A. Azam and M. Grätzel, *J. Electrochem. Soc.*, 1996, **143**, 3099–3108.
- 13 M. Shukla, N. Srivastava and S. Saha, *J. Mol. Struct.*, 2010, **975**, 349–356.
- 14 R. Katoh, M. Hara and S. Tsuzuki, *J. Phys. Chem. B*, 2008, **112**, 15426–15430.
- 15 H. Katayanagi, S. Hayashi, H. o Hamaguchi and K. Nishikawa, *Chem. Phys. Lett.*, 2004, **392**, 460–464.
- 16 Y. Umebayashi, H. Hamano, S. Tsuzuki, J. N. Canongia Lopes, A. A. H.

- Pádua, Y. Kameda, S. Kohara, T. Yamaguchi, K. Fujii and S.-i. Ishiguro, *J. Phys. Chem. B*, 2010, **114**, 11715–11724.
- 17 E. A. Turner, C. C. Pye and R. D. Singer, *J. Phys. Chem. A*, 2003, **107**, 2277–2288.
- 18 M. H. Ghatee, A. R. Zolghadr, F. Moosavi and Y. Ansari, *J. Chem. Phys.*, 2012, **136**, 124706.
- 19 M. H. Ghatee and Y. Ansari, *J. Chem. Phys.*, 2007, **126**, 154502.
- 20 P. D'Angelo, A. Zitolo, V. Migliorati, G. Mancini, I. Persson and G. Chillemi, *Inorg. Chem.*, 2009, **48**, 10239–10248.
- 21 V. Migliorati, G. Chillemi and P. D'Angelo, *Inorg. Chem.*, 2011, **50**, 8509–8515.
- 22 V. Migliorati, A. Zitolo, G. Chillemi and P. D'Angelo, *ChemPlusChem*, 2012, **77**, 234–239.
- 23 P. D'Angelo, G. Chillemi, V. Barone, G. Mancini, N. Sanna and I. Persson, *J. Phys. Chem. B*, 2005, **109**, 9178–9185.
- 24 G. Mancini, N. Sanna, V. Barone, V. Migliorati, P. D'Angelo and G. Chillemi, *J. Phys. Chem. B*, 2008, **112**, 4694–4702.
- 25 P. D'Angelo, A. Zitolo, V. Migliorati and I. Persson, *Chem.-Eur. J.*, 2010, **16**, 684–692.
- 26 V. Migliorati and P. D'Angelo, *RSC Adv.*, 2013, **3**, 21118–21126.
- 27 V. Migliorati, G. Mancini, S. Tatoli, A. Zitolo, A. Filippini, S. De Panfilis, A. Di Cicco and P. D'Angelo, *Inorg. Chem.*, 2013, **52**, 1141–1150.
- 28 P. D'Angelo, V. Migliorati, G. Mancini and G. Chillemi, *J. Phys. Chem. A*, 2008, **112**, 11833–11841.
- 29 V. Migliorati, G. Mancini, G. Chillemi, A. Zitolo and P. D'Angelo, *J. Phys. Chem. A*, 2011, **115**, 4798–4803.
- 30 P. D'Angelo, V. Migliorati and L. Guidoni, *Inorg. Chem.*, 2010, **49**, 4224–4231.
- 31 G. Chillemi, V. Barone, P. D'Angelo, G. Mancini, I. Persson and N. Sanna, *J. Phys. Chem. B*, 2005, **109**, 9186–9193.
- 32 V. Migliorati, A. Zitolo and P. D'Angelo, *J. Phys. Chem. B*, 2013, **117**, 12505–12515.
- 33 P. D'Angelo, A. Zitolo, G. Aquilanti and V. Migliorati, *J. Phys. Chem. B*, 2013, **117**, 12516–12524.
- 34 A. Filippini and A. Di Cicco, *Phys. Rev. B*, 1995, **52**, 15135–15149.
- 35 M. Nakakoshi, M. Shiro, T. Fujimoto, T. Machinami, H. Seki, M. Tashiro and K. Nishikawa, *Chem. Lett.*, 2006, **35**, 1400–1401.
- 36 W. Smith and T. Forester, *J. Mol. Graphics*, 1996, **14**, 136–141.
- 37 K.-S. Kim, B.-K. Shin and H. Lee, *Korean J. Chem. Eng.*, 2004, **21**, 1010–1014.
- 38 J. N. Canongia Lopes, J. Deschamps and A. A. H. Pádua, *J. Phys. Chem. B*, 2004, **108**, 2038–2047.
- 39 J. N. Canongia Lopes and A. A. H. Pádua, *J. Phys. Chem. B*, 2006, **110**, 19586–19592.
- 40 W. L. Jorgensen, J. P. Ulmschneider and J. Tirado-Rives, *J. Phys. Chem. B*, 2004, **108**, 16264–16270.
- 41 B. L. Bhargava and S. Balasubramanian, *J. Chem. Phys.*, 2007, **127**, 114510.
- 42 S. Nosé, *J. Chem. Phys.*, 1984, **81**, 511–519.
- 43 D. J. Evans and B. L. Holian, *J. Chem. Phys.*, 1985, **83**, 4069–4074.
- 44 U. Essmann, L. Perera, M. L. Berkowitz, T. Darden, H. Lee and L. G. Pedersen, *J. Chem. Phys.*, 1995, **103**, 8577–8593.
- 45 M. Brehm and B. Kirchner, *J. Chem. Inf. Model.*, 2011, **51**, 2007–2023.
- 46 M. Kohagen, M. Brehm, Y. Lingscheid, R. Giernoth, J. Sangoro, F. Kremer, S. Naumov, C. Iacob, J. Kärger, R. Valiullin and B. Kirchner, *J. Phys. Chem. B*, 2011, **115**, 15280–15288.
- 47 M. Kohagen, M. Brehm, J. Thar, W. Zhao, F. Müller-Plathe and B. Kirchner, *J. Phys. Chem. B*, 2011, **115**, 693–702.
- 48 M. G. Del Pópolo and G. A. Voth, *J. Phys. Chem. B*, 2004, **108**, 1744–1752.
- 49 X. Zhong, Z. Fan, Z. Liu and D. Cao, *J. Phys. Chem. B*, 2012, **116**, 3249–3263.